

Ground Motions Recorded in Rome during the April 2009 L'Aquila Seismic Sequence: Site Response and Comparison with Ground-Motion Predictions Based on a Global Dataset

by Arrigo Caserta, David M. Boore, Antonio Rovelli, Aladino Govoni, Fabrizio Marra, Giuseppe Della Monica, and Enzo Boschi

Abstract The mainshock and moderate-magnitude aftershocks of the 6 April 2009 M 6.3 L'Aquila seismic sequence, about 90 km northeast of Rome, provided the first earthquake ground-motion recordings in the urban area of Rome. Before those recordings were obtained, the assessments of the seismic hazard in Rome were based on intensity observations and theoretical considerations. The L'Aquila recordings offer an unprecedented opportunity to calibrate the city response to central Apennine earthquakes—earthquakes that have been responsible for the largest damage to Rome in historical times. Using the data recorded in Rome in April 2009, we show that (1) published theoretical predictions of a 1 s resonance in the Tiber valley are confirmed by observations showing a significant amplitude increase in response spectra at that period, (2) the empirical soil-transfer functions inferred from spectral ratios are satisfactorily fit through 1D models using the available geological, geophysical, and laboratory data, but local variability can be large for individual events, (3) response spectra for the motions recorded in Rome from the L'Aquila earthquakes are significantly amplified in the radial component at periods near 1 s, even at a firm site on volcanic rocks, and (4) short-period response spectra are smaller than expected when compared to ground-motion predictions from equations based on a global dataset, whereas the observed response spectra are higher than expected for periods near 1 s.

Online Material: Velocity models used in computing theoretical site response.

Introduction

It has long been thought that surficial geology underlying Rome should produce important spatial variations in the amplifications of seismic waves. For example, [Ambrosini *et al.* \(1986\)](#) concluded that the most severe damage within the city of Rome caused by a large earthquake in 1915, near Avezzano in the Apennines and 80 km from Rome, occurred to buildings located on the Holocene alluvial fill of the Tiber valley. In addition, [Boschi *et al.* \(1995\)](#) and [Moczo *et al.* \(1995\)](#) concluded that historical monuments erected on soft layers have been affected by earthquake shaking. Studies aimed at quantifying the effects of local geology, including 2D modeling using finite-difference techniques as well as a hybrid technique based on mode summation and 2D finite differences, have been conducted since the early 1990s ([Fah *et al.*, 1993](#); [Rovelli *et al.*, 1994, 1995](#)). 3D models, limited to a maximum frequency of 1 Hz, were performed for the city of Rome by [Olsen *et al.* \(2006\)](#). More recently, a multidisciplinary research project dealt with the physical and mechanical properties of the different Holocene sediments

in the Tiber valley and the underlying Plio-Pleistocene material ([Bozzano *et al.*, 2008](#)). The project involved the installation of a permanent seismic array and a classification of the physical and mechanical properties of the rocks constituting the geological subsoil of Rome, under both static and dynamic conditions (investigations of the near-surface material and installation of seismic arrays has now been extended to tributary lateral valleys of the Tiber River [[Caserta *et al.*, 2012](#)]). 1D numerical models of local seismic response to possible strong motion in the city of Rome were performed, stressing the important role that an up to 60-m-thick silty-clayey sedimentary sequence inside the Tiber alluvia has on ground-motion amplification for realistic seismic inputs ([Bozzano *et al.*, 2008](#)). None of the studies just mentioned used recordings of ground motions in Rome, as the high level of cultural noise in the urban area and the low seismicity around Rome precluded the collection of usable motions from earthquake sources. The April 2009 sequence of earthquakes in L'Aquila, about 90 km from Rome, changed this.

The data collected during the April 2009 seismic sequence are the first instrumental earthquake data ever recorded in the city of Rome, and they allow us to check previous theoretical estimates of the seismic response of Rome, thus providing some observational basis for the seismic hazard assessment of the city.

In this article we first discuss similarities and differences of the recordings of the L'Aquila mainshock at two sites, one in the Tiber valley and one on the uplands adjacent to the valley. We then compare observed and theoretical calculations of the relative site response at the two sites, as well as the ratio of motions at the Tiber valley site at the ground surface and in a borehole 72 m beneath the ground surface. Finally, we compare the motions from the mainshock to motions from the Pacific Earthquake Engineering Center Next Generation Attenuation ground-motion prediction equations (GMPEs) derived from a global set of data.

Recordings of the L'Aquila Earthquakes: Site Information and Mainshock Record Characteristics

Site and Data Information

Although the early settlements of ancient Rome were established on the famous “Seven Hills”, the city expanded over the large alluvial plain of the Tiber River and those of its tributaries (Fig. 1), and more than one-half of the historical center is built over these fluvial deposits. Similarly, a large part of the most recently built portion of the city is located above more than 50 m of alluvium deposited by a network of Holocene streams. This stream network originated during the Würm glacial epoch (lasting until 18 ka before present) through re-incision and deepening of the valleys that had developed during previous glacial-interglacial periods (Marra *et al.*, 2008). The role of these lateral variations on ground motions felt in Rome by the population during earthquakes is discussed in Cifelli *et al.* (2000) and Sbarra *et al.* (2012). The sediments filling the incision of the Tiber River within the city of Rome consist of a fining-upward succession, with a 6–8-m-thick level of gravel at the base, overlain by a 50–60-m-thick sequence of sand and clay (Bozzano *et al.*, 2000). A schematic cross section between the two stations used in this article showing the subsurface geologic conditions is given in Figure 2. This upper sequence of sand and clay is characterized by normally to weakly overconsolidated clay-sandy silt, saturated in water, with low deformability moduli (Bozzano *et al.*, 2000). Within the central axis of the Tiber River valley, the material beneath the alluvial sediments is a marine Plio-Pleistocene sequence (Marra and Rosa, 1995), consisting of alternating, decimeter-thick levels of clay and sand, with an overconsolidation ratio > 5 and low compressibility (Bozzano *et al.*, 2008). This Plio-Pleistocene clayey substrate is about 900 m thick in the study area (as indicated by a deep drilling performed in 1935 in downtown Rome [Signorini, 1939]), during which the silicic-carbonatic Cenozoic succession (which constituted the bottom of the

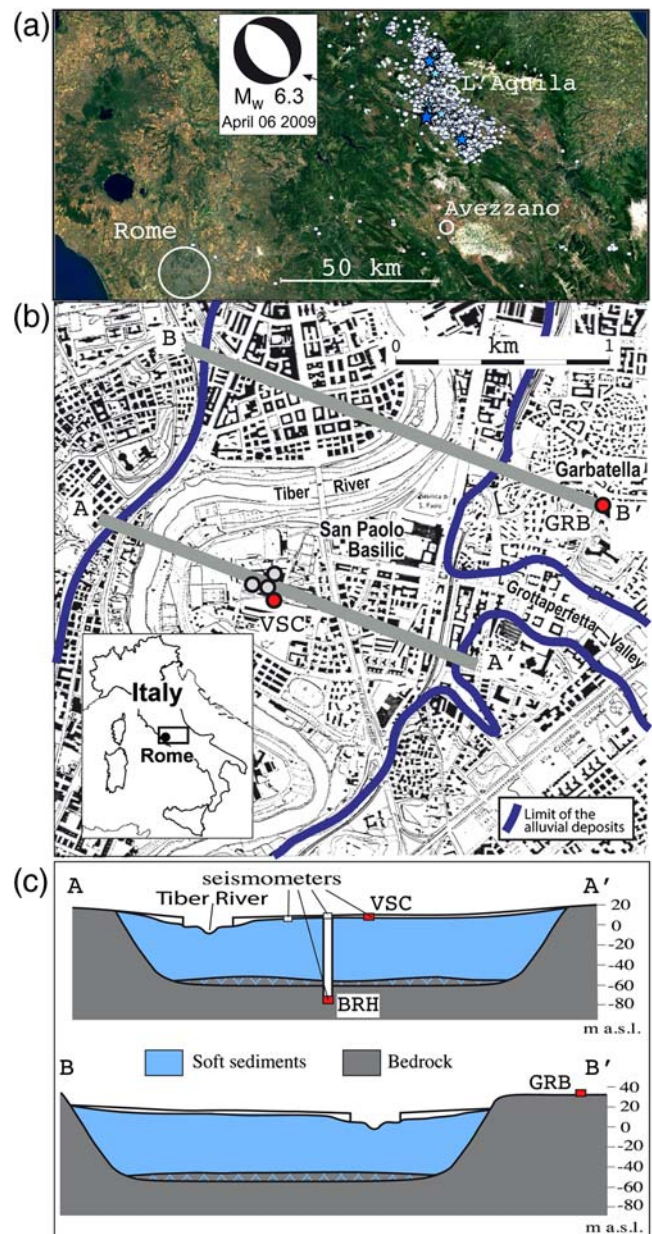


Figure 1. (a) Epicenters (small circles) of the April 2009 seismic sequence in the central Apennine mountain chain. The mainshock (the black arrow near L'Aquila) is about 90 km from Rome; its focal mechanism is from Herrmann *et al.* (2011). (b) Map of the study area of Rome showing seismological stations (circles) that have been in place since 2008; stations with red circles are those used in this study. (c) Transversal cross sections of the Tiber valley: AA' is through the surface station VSC and the 72-m deep borehole station (BRH) in the Tiber valley; BB' is through GRB, on volcanic rock. The descriptors “soft sediments” and “bedrock” are generic terms meant to signify materials with low and high stiffness, respectively; the true bedrock is limestone, at a depth near 900 m (as shown in the next figure). The color version of this figure is available only in the electronic edition.

Pliocene sea basins; Funiciello and Parotto, 1978), was encountered 917 m below the present-day sea level. The upper portion of the valley sides, as well as the land away from the alluvial plains, where the rest of the city is built, are

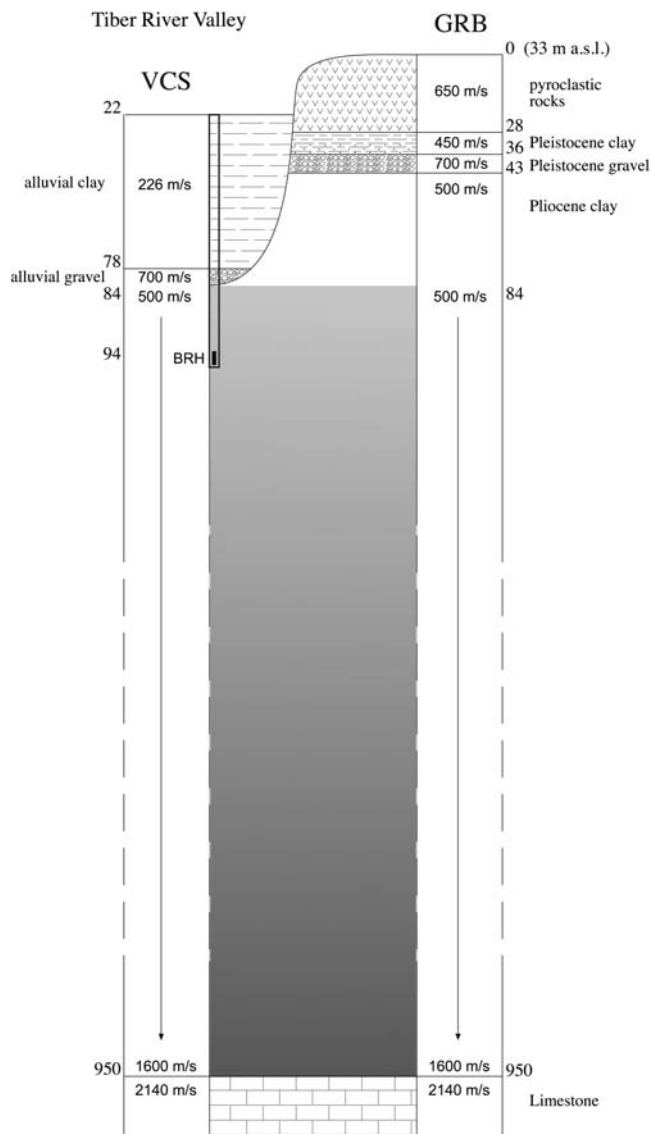


Figure 2. Schematic cross section from VCS to GRB. VCS is underlain by about 50 m of clays with an average shear-wave velocity of 226 m/s, followed by stiffer material, including an 8-m-thick gravel layer with a velocity of 700 m/s; see Appendix A and (E) the electronic supplement for details.

composed of Pleistocene fluvial deposits (the Paleo-Tiber unit; see Marra and Rosa, 1995, and Florindo *et al.*, 2007), comprising a 10-m-thick layer of coarse gravel overlain by consolidated sandy clay, and this in turn is overlain by a thick volcanic cover, represented by more or less lithified pyroclastic-flow deposits and alternating ash-fall deposits (Kärner *et al.*, 2001), partially intercalated into the continental sedimentary deposits (Kärner and Marra, 1998).

Since early 2008, a small-aperture four-station array has operated on the alluvial sediments within the Tiber River valley in Valco San Paolo, in the southern part of the historical sector (Fig. 1). The distance between the array stations is less than 100 m, all of them are equipped with three-component 5-s velocity transducers, and the horizontal components are

oriented north–south and east–west. Data are sampled at a rate of 1000 Hz, using 24-bit analog-to-digital converters, and time synchronism is provided by a Global Positioning System system at each station. In this paper, we use records from one of the array stations (VSC) and another station (GRB) installed about 2 km east of the array (by coincidence, both stations are close to a line from the L’Aquila region to the Tiber River valley stations). GRB lays above the Pleistocene pyroclastic sequence and the underlying, older sedimentary deposits of the Paleo-Tiber River (Marra and Rosa, 1995). VSC and GRB provided good-quality acceleration time histories during the L’Aquila seismic sequence, being also equipped with acceleration transducers.

In addition to the surface stations just described, one three-component short-period (1 s) seismometer is installed at the bottom of a 72-m-deep borehole, within the Plio-Pleistocene clayey rock, 15 m below the base of the alluvial soft sediments at Valco San Paolo; we designate recordings from this sensor as coming from station BRH. The BRH motions were converted to acceleration time series by deconvolving the velocity-sensor response; this deconvolution was noisy for frequencies below about 0.5 Hz, and therefore we only use the BRH data for frequencies above 0.5 Hz. The borehole data are continuously recorded at the surface using the same acquisition system as used for the stations deployed at the surface. In this article, we analyze data from the main-shock, as well as from nine aftershocks; Table 1 gives information about the events.

Features of the Recordings

Before showing the time series at the recording sites, we first discuss the smoothed Fourier acceleration spectra (FAS) at the three stations, shown in Figure 3, because most of the main findings of our study are evident in the relative shapes and amplitudes of the FAS. The horizontal motions from which the FAS were computed have been rotated into radial (R) and transverse (T) directions, using a station-to-source azimuth of 53°. The figure shows that the horizontal-component motions are larger than the vertical-component motions for frequencies less than about 5 Hz. At both GRB and VSC, there is a peak in the FAS of the radial components for frequencies near 1 Hz and the region of elevated FAS is broader at GRB than at VSC. A distinct difference in the VSC and GRB FAS in the region of the maximum FAS is that the transverse component FAS is much smaller than the radial component FAS at GRB, while at VSC the FAS from the two horizontal components are comparable. At GRB the radial component FAS is generally larger than the transverse-component FAS for frequencies less than 0.2 Hz. At both GRB and VSC the FAS from the two horizontal components are similar for frequencies greater than a few Hz.

Figure 4 shows a direct comparison of acceleration and velocity time series for the surface (VSC) and downhole (BRH) sensors. The VSC motions are much larger than the BRH motions. This is expected for several reasons: (1) the

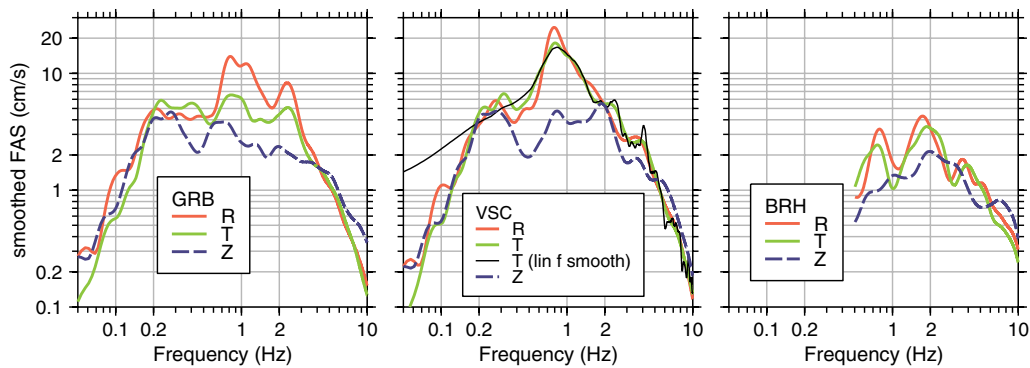


Figure 3. Fourier acceleration spectra (FAS), smoothed using [Konno and Ohmachi \(1998\)](#) smoothing over logarithmic frequency, with their smoothing parameter set to $b = 20$. For comparison, smoothing over equally spaced frequencies with a triangular smoothing window with base of 0.5 Hz is shown for the T component at VSC (lin f smooth). The spectra were computed from unfiltered acceleration time series, using a 200 s window. A lower frequency limit of 0.5 Hz is used for BRH because the conversion of the 1-Hz velocity sensor motion to acceleration was noisy below that limit. The color version of this figure is available only in the electronic edition.

VSC recordings are at the surface, and thus constructive interference of the incident and reflected waves will amplify the motions by a factor of about 2 (relative to the incident motions); (2) the lower shear-wave velocities will lead to an amplification of the waves as they proceed up the soil column, due to conservation of energy; (3) resonance of the waves reverberating in the sedimentary layers will produce additional amplification at the fundamental frequency and at the overtone frequencies; and (4) the BRH instrument is installed near a large change in seismic-wave impedance, where destructive interference of up- and downgoing waves will lead to reduced motions ([Joyner et al., 1976](#); [Shearer and Orcutt, 1987](#); [Bindi et al., 2010](#); [Kinoshita, 2010](#)). Quantitative evaluations of these effects in the BRH record are discussed in the [Site Amplification at VSC and GRB](#) section.

Time series of ground acceleration, velocity, and displacement at VSC and GRB are shown in [Figure 5](#) for transverse (T), radial (R), and vertical (Z) components. Comparison between VSC and GRB indicates a substantial similarity of displacement waveform shapes and amplitudes, with VSC being somewhat larger than GRB on the T component. The dominant frequency of the displacement time

series is near 0.2 Hz, so these graphs indicate that there is little relative site response at low frequencies. There is less agreement in waveform shapes and amplitudes for the velocity and acceleration time series than for the displacement time series, and for those motions VSC is much larger than GRB on the T component. These graphs suggest that there is relative site response at higher frequencies, at least for the T component (spectral ratios will be used later to quantify the site response). There is also a significant difference in the displacement waveforms for the R and T components throughout the records, including the occurrence of a distinct *P* arrival on the R component that is not present on the T component. The *P* arrival on the R component and the overall dissimilarity of the R and T motions indicate that the rotations of the horizontal components have succeeded in separating the *SH* and the *P-SV* phases, at least for the lower-frequency motions.

A puzzling feature of the GRB–VSC comparison is the relatively large T-component motion at VSC. We expect from the theoretical radiation pattern that the transverse shear-wave motion should be near nodal for waves propagating from the source to Rome, and thus the radial component

Table 1
Date and Source Parameters of Earthquakes Analyzed in This Study

Event	yyyy/mm/dd/	hh:mm:ss (UTC)	Latitude (° N)	Longitude (° W)	Depth (km)	M (CMT)	M (Hea11)*
1	2009/04/06	1:32:39	42.334	13.334	5	6.3	6.1
2	2009/04/06	2:27:46	42.375	13.342	10	—	4.1
3	2009/04/06	2:37:04	42.366	13.340	10	—	4.8
4	2009/04/06	7:17:10	42.355	13.367	9	—	4.0
5	2009/04/06	16:38:09	42.362	13.333	10	—	4.3
6	2009/04/06	23:15:37	42.451	13.364	7	—	4.9
7	2009/04/07	9:26:28	42.342	13.388	10	—	4.7
8	2009/04/07	17:47:37	42.275	13.464	16	5.5	5.4
9	2009/04/07	21:34:29	42.380	13.376	7	—	4.2
10	2009/04/09	19:38:16	42.501	13.356	7	—	5.0

*Hea11 are seismic moments from [Herrmann et al. \(2011\)](#). See [Data and Resources](#) for the web availability of hypocenter determination and moment magnitude.

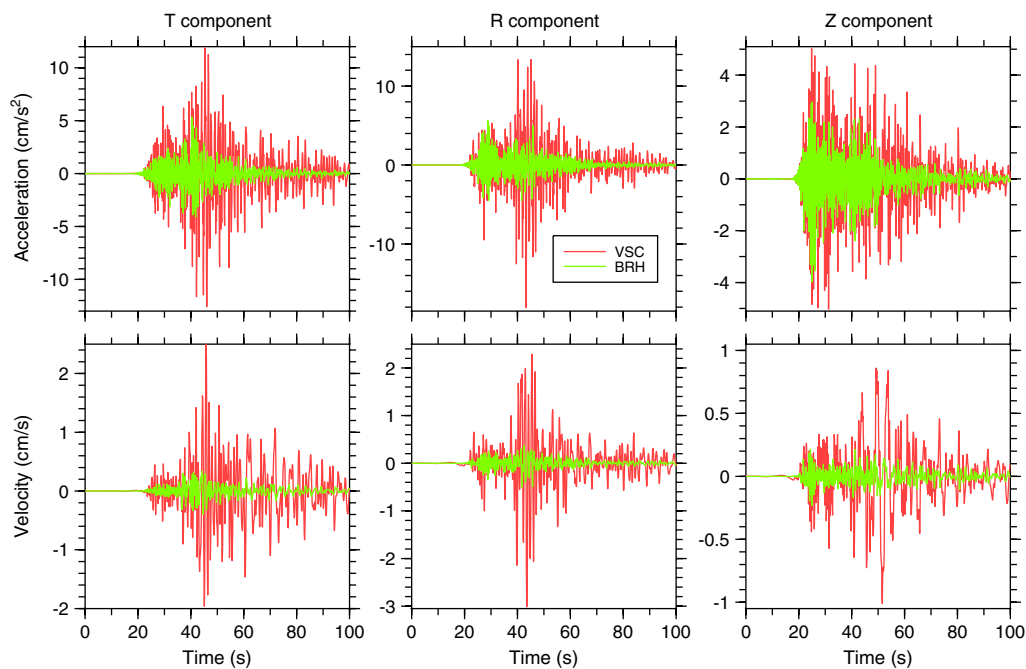


Figure 4. Direct comparison of acceleration and velocity time series for the surface (VSC) and downhole (BRH) sensors. The velocity time series were obtained by integration of accelerations filtered with acausal 0.1- and 10-Hz filters which decayed as f^8 at low frequency and f^{-8} at high frequency. The displacement time series are not shown because of concern that the low-frequency motions at BRH, obtained from the 1-Hz velocity sensor at BRH, may not be accurate. The color version of this figure is available only in the electronic edition.

should dominate the motion. This is true for GRB, but not for VSC, at least at frequencies less than 4 Hz (except for the 0.2–0.5 Hz band; see Fig. 3). To look into the increased T-component motion at VSC relative to that at GRB in more detail, we show in Figure 6 hodograms of the two components of horizontal motion, where we have band-pass filtered the accelerations between 0.6 and 1.1 Hz (this range was chosen so as to encompass the peak in the FAS of the R and T components at VSC). The motions at GRB and VSC are close to being linearly polarized in the radial direction for times before about 44.5 s; this agrees with expectations from the radiation pattern of the earthquake. Beyond about 44.5 s, the motions tend to become elliptically polarized (in the horizontal plane), but both components of horizontal motion for the later times are much larger at VSC than at GRB. Looking closely at the filtered time series, the R motions at GRB start to decay in amplitude beyond about 44 s, but those at VSC stay high for several more cycles. In addition, the T component grows in amplitude at VSC for times greater than 44 s, unlike the T-component motion at GRB; this leads to the peak in the VSC FAS for the T component. Some of the increase duration of the motion at VSC is undoubtedly due to fundamental resonance in the sediments underlying VSC, but the relative increase in the T component later in the record suggests some complicated wave propagation in the short distance between GRB and VSC. Lateral refraction of the waves as they enter the Tiber River valley could also account for apparent increase in the T component at later times.

Site Amplification at VSC and GRB

Observations

Estimates of relative amplification between GRB and VSC are given by ratios of the FAS from both sites, but these ratios say nothing about the station-specific amplifications. For VSC and BRH, the ratios of FAS provide a measure of station-specific amplification at VSC relative to the motion at BRH, which is located somewhat below the large velocity change between the Holocene and Pliocene sediments (see Fig. 2). Having no borehole recordings at GRB, it is not possible to have a direct estimate of the station-specific amplification at that station. A number of studies, however, have concluded that the frequencies of resonant peaks at a site can be reliably determined using horizontal-to-vertical spectral ratios (HVSr), particularly for those sites with a large impedance contrast in layers not far from the surface even though the amplitude of the HVSr at the resonant frequencies might not be a good estimate of the site response (e.g., Lermo and Chávez-García, 1993; Konno and Ohmachi, 1998; Fäh *et al.*, 2001; Bonnefoy-Claudet *et al.*, 2008). We show in Figure 7 both types of site response estimates. The graphs in the top row show HVSr for the mainshock recordings at GRB and VSC, while the two graphs in the bottom row show the VSC/BRH and VSC/GRB relative site response. These two lower graphs include ratios from the mainshock recordings, as well as the average of the ratios from nine aftershocks (see Table 1). To provide more information about the sensitivity of the HVSr to the component of horizontal motion and to

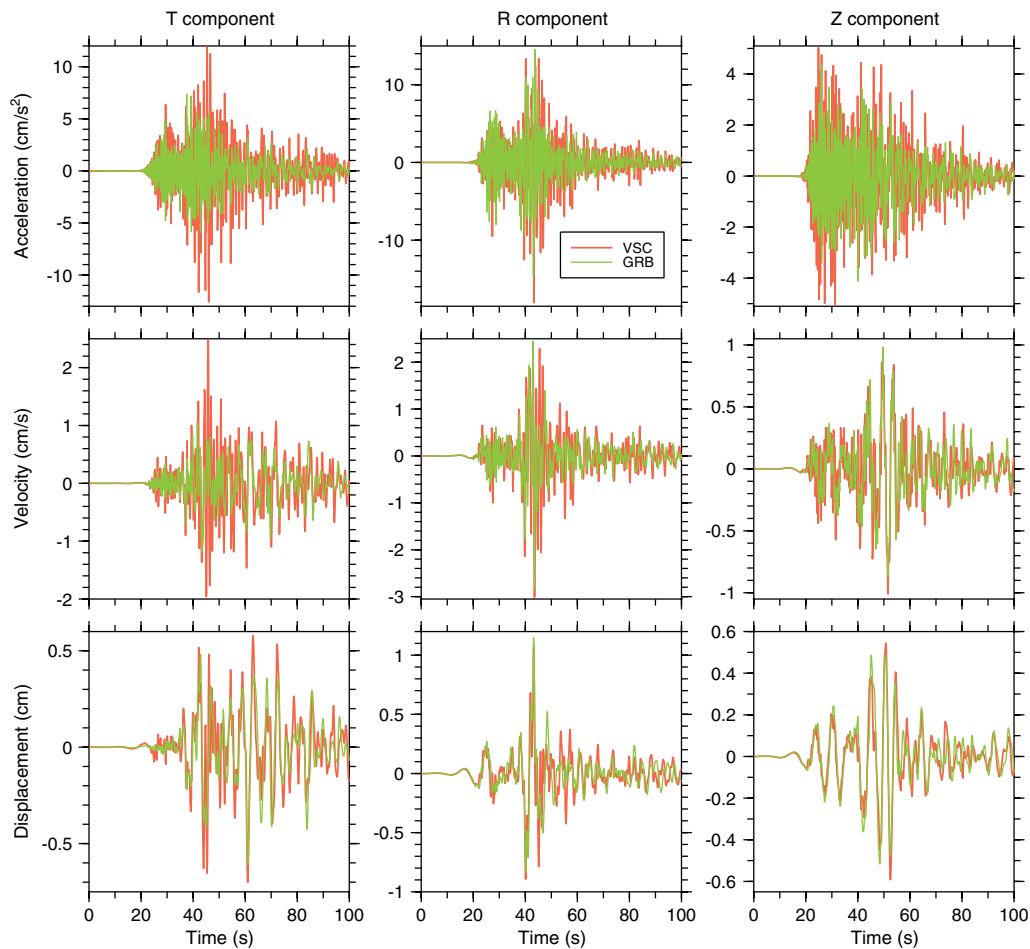


Figure 5. Direct comparison of acceleration, velocity, and displacement time series at VSC and GRB. The velocity and displacements were obtained by integration of accelerations filtered with acausal 0.1- and 10-Hz filters which decayed as f^{-8} at low frequency and f^{-8} at high frequency. The GRB time series have been shifted by a constant amount for all components (an 0.8-s delay) so that the displacements traces are approximately time-aligned with the VSC displacements. The color version of this figure is available only in the electronic edition.

the types of motion, we show in Figure 8 shaded contour maps of HVSR for the mainshock, the aftershocks, and noise as a function of direction of horizontal ground motion and frequency. In constructing Figure 8 we rotated the two recorded horizontal motions at a station into a specific azimuth. The HVSR was then computed for this rotated motion, the results were repeated for a range of azimuths from 0° to 180° , clockwise from north, and the shaded contour map was constructed.

The HVSRs in Figures 7 and 8 show a strong peak at frequencies somewhat greater than 1.0 Hz at GRB and less than 1.0 Hz at VSC. Additional peaks at other frequencies are present for the aftershock averages. For the mainshock and the aftershock average the peak HVSR near 1.0 Hz at GRB corresponds roughly to radial motion (the station to source azimuth is about 53° – 56° , depending on station and which part of the fault was used as the source location), which is consistent with expectation from the faulting mechanism that the radial component should be dominant for waves propagating to Rome. At VSC the peak HVSR for

the mainshock tends to be at larger azimuths than at GRB, which is probably a consequence of the increased motion on the transverse component discussed earlier. The HVSR for the noise is less sensitive to azimuth, again as expected, since the noise will be arriving at the stations from many azimuths, unlike the motions from the L'Aquila earthquakes. The peak frequencies of the HVSR from the noise (1.11 Hz for GRB and 0.94 Hz for VSC) are similar to those from the L'Aquila events, but the peak amplitudes are smaller by a factor of 2–3. In addition, the peak response at GRB from the noise HVSR is only about half that at VSC.

If we accept peaks in HVSR as being due to station-specific site response, then the graphs in Figure 8 indicate a pronounced site response at a frequency near 1 Hz, both on the low-velocity sediments in the Tiber River valley (VSC), as well as on the nearby uplands (GRB). The presence of a strong site response at VSC is not a surprise, but we did not expect a resonant-like site response at GRB. An additional complexity in inferring site response from the average-aftershock HVSR at GRB is the presence of four peaks in the

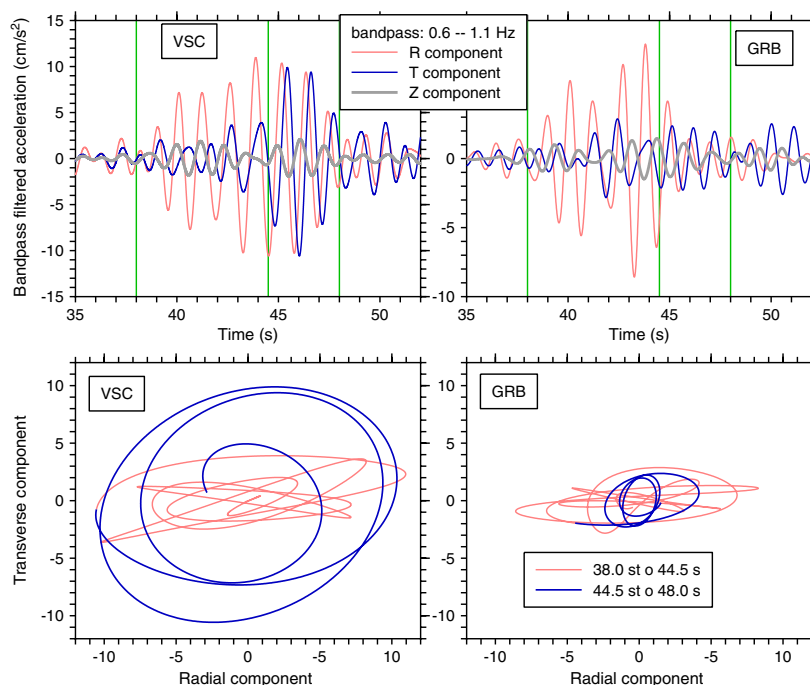


Figure 6. Band-pass-filtered accelerations at VSC and GRB (top row) and hodograms for the indicated time intervals (the time intervals are indicated by the vertical lines in the top row of graphs). For completeness, the vertical component band-pass-filtered accelerations are also included in the top graphs. The GRB time series have been shifted by 0.8 s so that they are time aligned with the R component at VSC for times near 40 s. The color version of this figure is available only in the electronic edition.

HVSR; if these indicate site resonances, why do they not occur for either the mainshock or the noise? Moreover, there is a small difference in the frequencies of the peak HVSR from the noise and from the mainshock and aftershock recordings. This could be due to the different wavefield structure between noise and earthquakes, including different percentages of Love and Rayleigh waves in the motions (Bonnefoy-Claudet *et al.*, 2008). We consider the HVSR from the noise to be the best indicator of an overall average response at the sites.

To quantify the relative amplification between the Holocene alluvial deposits under VSC and the Pleistocene pyroclastics beneath GRB, we computed Fourier spectral ratios for the T and R components; these are shown in the lower two graphs in Figure 7. We only show ratios for the horizontal components because our main interest is in the site response of those components. Spectral ratios were computed for an individual event (the mainshock), and for the geometric mean over a subset of nine of the strongest aftershocks (Table 1, events 2 through 10) selected as having a satisfactory signal-to-noise ratio (higher than 3 in the frequency band 0.5–8 Hz). For the nine aftershock spectral-ratios we converted the velocity-transducer seismograms of stations VSC, BRH, and GRB to acceleration time series, from which we computed Fourier spectra. All spectra were smoothed before the ratios were computed. Because we expected to see higher modes in the VSC/BRH ratios, at roughly equispaced frequencies, we used a triangle smooth-

ing operator with a frequency-independent width of 0.5 Hz; smoothing using an operator whose width is proportional to frequency (e.g., the Konno and Ohmachi, 1998, smoothing) tends to smear out higher modes (compare the T component FAS for VSC in Fig. 3). In contrast, in the FAS shown in Figure 3 we used a smoothing operator whose width is proportional to frequency, as this operator produces less distortion at low frequencies (and in Fig. 3 we wanted to show that the FAS at low frequencies are similar for both VSC and GRB, indicating no difference in the long-period site response at the two stations). Near the fundamental mode frequency of 1 Hz there is little difference between using the two smoothing operators. For both VSC/BRH and VSC/GRB we used a log-frequency axis to emphasize the fundamental mode, and a log-amplification axis to accentuate the higher modes (which have smaller amplitudes than the fundamental mode).

The VSC/BRH ratios are all quite consistent and show a series of modes with the dominant peak in the ratio at 1 Hz presumably being a fundamental mode (this is confirmed by the theoretical amplifications shown later), and higher modes at frequencies of about 2.9, 4.5, 6.1, 7.8, and 9.7 Hz. The frequency of the fundamental mode is somewhat higher than the frequency of the peak FAS and the peak HVSR at VSC (close to 0.8 Hz); this is because the BRH FAS also has a peak at 0.8 Hz and a minimum at 1.05 Hz, the combination of which produces an apparent shift in the frequency of peak in the VSC/BRH ratio.

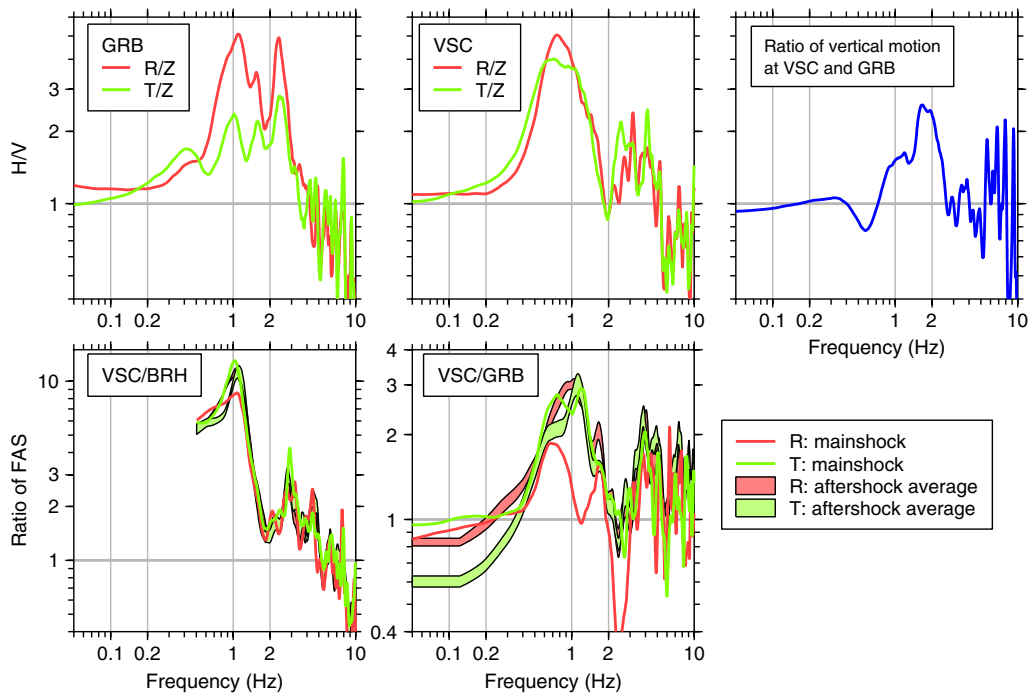


Figure 7. Top row: ratios of smoothed whole-record horizontal to vertical Fourier acceleration spectra at GRB and VSC. Bottom row: ratios of smoothed Fourier acceleration spectra for indicated sites. The shaded regions for the aftershock averages span the 68% confidence limits of the mean values of the ratios. As discussed in the text, the VSC/BRH ratio is not plotted for frequencies less than 0.5 Hz because the BRH recordings might not be trustworthy for lower frequencies. Smoothing was done over equally spaced frequencies using a triangle operator with a base width of 0.5 Hz. The color version of this figure is available only in the electronic edition.

For the VSC to GRB relative site response (Fig. 7, lower right graph), the ratios of the R and T components for the mainshock are dissimilar, unlike the R and T component ratios for VSC/BRH (Fig. 7, lower left graph). Some oscillations in the GRB mainshock FAS (see Fig. 3) lead to com-

plexity in the VSC/GRB ratios, but the differences in the R and T component ratios for the mainshock have more to do with the time-varying differences of the R and T components demonstrated in Figure 6. In contrast to the mainshock motions, the ratios of the average aftershock motions are similar

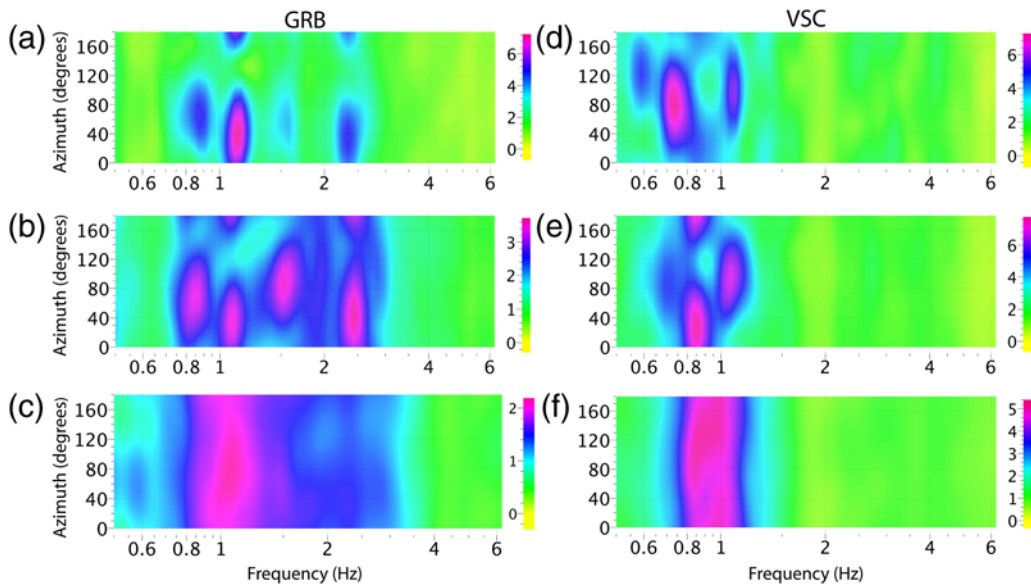


Figure 8. (a,d) Horizontal-to-vertical spectral ratios (HVSR) from the mainshock, (b,e) average of nine aftershocks, (c,f) and noise. The horizontal component was obtained by rotating the observed components into the azimuth shown on the ordinate scale. The spectra used in the ratios were smoothed over logarithmically spaced frequencies. The color version of this figure is available only in the electronic edition.

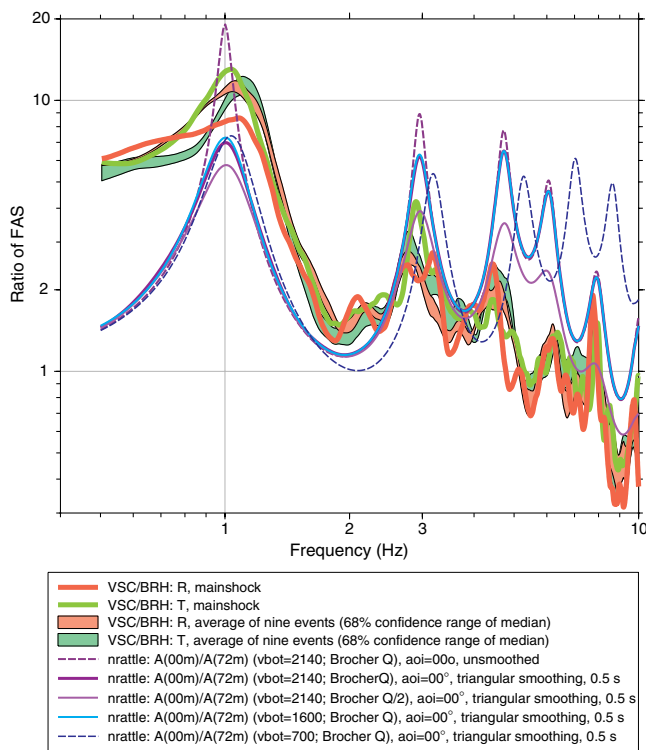


Figure 9. Observed and theoretical VSC/BRH ratios of FAS. Shown are ratios for the mainshock (for R and T separately) and for an average of nine aftershocks. With one exception (indicated in the legend), all ratios were formed from smoothed FAS, where the smoothing was over equally spaced frequencies, using a triangular weighting function with a base width of 0.5 Hz. The color version of this figure is available only in the electronic edition.

for the R and T components. We suggest that the VSC/GRB ratios based on nine aftershocks might be better measures of the average relative site response than the ratios from the recorded mainshock motions. The difference we find between ratios of motions from nearby sites for an individual event and from the average of multiple events has been observed from other studies (e.g., Chavez-Garcia *et al.*, 2000; Boore, 2004). Apparently small differences in focal mechanism, source-to-station azimuth, and propagation path can have a surprisingly large influence on spectral ratios for stations separated by only a few kilometers (but recall the consistency of the VSC/BRH ratios, so that very closely located stations should have similar ratios for similar components from events in the same geographic region, an unsurprising conclusion).

Predictions

Figures 9 and 10 also show a comparison between observed and theoretical amplifications at VSC, relative to GRB and to BRH. Most of the theoretical curves were computed using the program *nrrattle*, which assumes *SH* motion. A few amplifications shown in Figure 9 used the program *roll*, which assumes incident *SV* waves and includes *SV* to *P*-wave conversions. Both *nrrattle* and *roll* are included in the SMSIM package (Boore, 2005). The programs assume linear

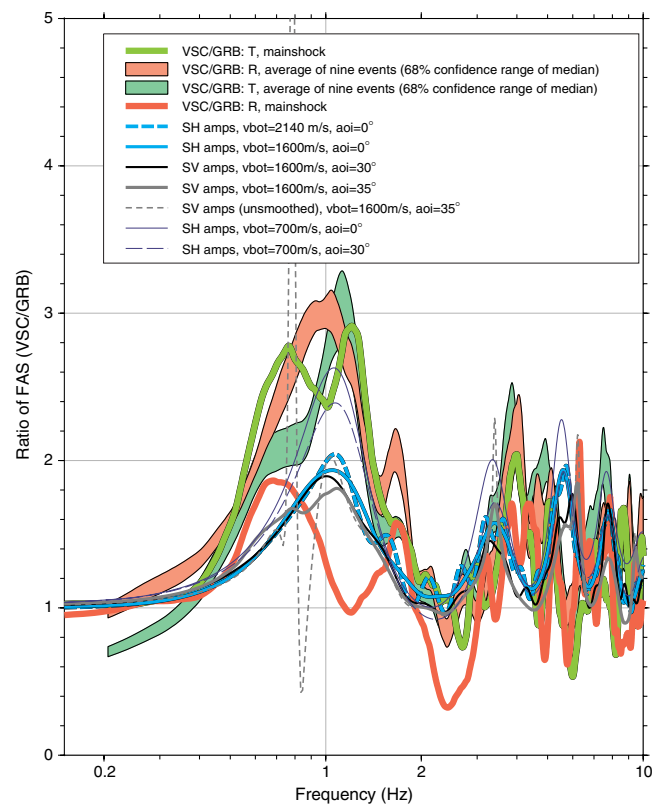


Figure 10. Observed and simulated VSC/GRB ratios of FAS. Shown are ratios for the mainshock (for R and T separately) and for an average of nine aftershocks. All ratios but one were formed from smoothed FAS, where the smoothing was over equally spaced frequencies, using a triangular weighting function with a base width of 0.5 Hz. Note that the ordinate scale is different here than in Figure 9. The color version of this figure is available only in the electronic edition.

elasticity and horizontal constant-velocity layers. They include the constructive and destructive interference of all reverberations. The details of the 1D shear-wave velocity models at the two sites are described in the Appendix A, the vertical profiles of VSC and GRB differing only in the upper layers above the clay rock of Rome (see Figs. 2 and A1). The shallower parts of the shear-wave velocity profile beneath VSC control the relative VSC and BRH amplification, and these shallow velocities are based on measurements in the borehole. In contrast, no measured velocities are available at GRB, and thus the velocity profile used in the calculations is based on judgment. After developing the profile, we discovered the apparent amplification at GRB near 1 Hz, based on the HVSR analysis. The profile in the Appendix A will not produce a strong resonance at that frequency. We chose not to modify that profile to produce a resonance near 1 Hz, however, as there would be little basis for choosing among the many profiles that could be constructed to give a 1-Hz resonance (and the noise HVSR indicates that the site amplification is rather small). In reading the following, please keep in mind that the predictions of the VSC/BRH will be much better determined than for VSC/GRB. We show the latter

because the overall comparison is in fact not unreasonable, and we use the VSC/GRB comparison to illustrate the dependence of the theoretical ratios on the angle of incidence, type of input motion, and choice of half-space velocity.

For the spectral ratio VSC/BRH (Fig. 9) the theoretical curves were obtained by dividing the *nrattle* response for a depth of 00 m (VSC) by the one for a depth of 72 m (BRH), using the VSC velocity model (this duplicates the actual procedure used to obtain the observed ratio; no extra factors of 2 were applied to either the observed or the theoretical ratios). Although not shown here, the theoretical ratios are not sensitive to the angle of incidence or to the details of the deeper part of the velocity model. Theoretical amplification curves are shown for two Q models (one with Q one-half that of the standard model, to see if a lower Q would give a better match to the observed amplification at higher frequencies). The theoretical curves are shown without smoothing and with the smoothing used for the amplification from the observations. Note that the sharpness and amplitudes of the theoretical amplification peaks are a consequence of the perfect constructive and destructive interference of the many reverberations within the sediment layers (e.g., as discussed in the appendix to [Boore and Joyner, 1991](#)). In reality, we expect lateral non-uniformity of the layers to cause the reverberations to arrive at times that are not exact multiples of the predicted travel time through the layers, and this, as well as scattering of the multiple arrivals, will tend to reduce the resonant peaks. For these reasons we would be surprised if we found excellent agreement between the observed and theoretical ratios. In general, there is good agreement in the frequencies of the fundamental and the high modes, and the gross comparison of observed and theoretical ratios is reasonable, given the considerations above.

Figure 10 shows a comparison of the observed and theoretical relative amplifications at VSC and GRB. We used a linear amplification axis so that the low amplitude ratio for the R component from the mainshock at a frequency of 2.4 Hz does not dominate the plot. The amplification at each station is relative to an effective rock surface recording that would be obtained by stripping off the layers above the half-space for each model. The VSC/GRB ratio was computed frequency by frequency. The theoretical amplifications were computed for vertical (0°) and oblique (30°) incidence for incident *SH* waves and 30° and 35° incidence for *SV* waves (incidence of 0° for *SV* waves is the same as for *SH* waves). The amplifications for incident *SH* waves are not very sensitive to incidence angle, but this is not true for *SV* waves when the incidence angle exceeds 30° . This is because at these angles the horizontal slowness of the incident *SV* wave exceeds the *P*-wave slowness in some of the layers, so that the angle of refraction becomes complex. This leads to large variations with frequency in the theoretical amplifications, as shown in Figure 10, and this might be a partial explanation for the unusual behavior of the R-component VSC/GRB ratio from the mainshock shown in Figure 7. Theoretical amplifications were computed for the complete model for VSC

and GRB discussed in Appendix A (with a 2400 m/s half-space) and with models truncated at depths corresponding to velocities of 700 and 1600 m/s in the complete models (with the portions of the complete models below those depths being replaced with 700 and 1600 m/s half-spaces). We used models with half-spaces shallower than that for the complete models because the amplifications for the complete models had numerous small amplitude oscillations over most of the frequency range; these occur at different frequencies for the VSC and the GRB (unlike the VSC and BRH simulations), and thus appear as oscillations in the VSC/GRB ratio riding on the more pronounced oscillations due to differences in the shallower parts of the velocity profiles. These oscillations are a consequence of the perfect constructive and destructive interference of waves reverberating through the whole section above the large impedance contrast at the base of each model (a step change in shear-wave velocities from 1593 to 2140 m/s), and we do not expect these oscillations to exist in more physically realistic models. The oscillations disappear when the half-space is taken to have a shear-wave velocity of 1600 m/s, which is close to that of the material just above the actual half-space in the unmodified models. We noticed that better agreement between the ratios from observations and simulations occurs if the half-spaces are taken to be at a relatively shallow depth, where the gradient part of the models in Figure A1 reaches a shear-wave velocity of 700 m/s. As we do not know the actual profile beneath either VSC (below about 70 m) or GRB, we assumed that the deeper parts of the profiles were the same. In summary, the results shown in Figure 10 indicate that the theoretical VSC/GRB ratios are in rough agreement with the observed VSC/GRB ratios, particularly for the T-component ratio from the mainshock recordings and the R and T ratios from the average of nine aftershock recordings. Both types of ratios indicate a fundamental mode amplification around 1 Hz, with the VSC motion being larger than the GRB motion by a factor of 2–3. They also both show a relative null in the amplification for frequencies near 2.4 Hz. The predicted frequencies of the higher modes are somewhat lower than the observed frequencies, which might indicate that the GRB velocity model needs refinement (recall that only the model for VSC at depths less than 62 m is based on measurements, and Fig. 9 shows that the frequencies of the observed and predicted modes are in good agreement for the fundamental and first few higher modes).

Comparison of L'Aquila Mainshock Motions in Rome with Other L'Aquila Recordings and with Predictions from GMPEs Based on Global Datasets

To see if the motions recorded in Rome from the L'Aquila mainshock are representative of motions at this distance from earthquakes with *M* 6.3, in this section we make two comparisons: (1) response spectra from the GRB recordings with response spectra from three other L'Aquila mainshock recordings at a similar epicentral distance and average

near-surface shear-wave velocity, but different azimuths, and (2) response spectra from GMPEs based on a large global dataset. Figure 11 contains the comparisons, where the seismic intensity measure is GMRotI50, an orientation-independent measure of 5%-damped response spectral acceleration (PSA) computed from horizontal ground motion, similar to the geometric mean, as discussed in Boore *et al.* (2006). The PSAs for the radial and transverse components are also shown. Many of the features in the response spectra from the mainshock recordings were seen previously in the FAS plots (Fig. 3). These include the pronounced peak at 1.25 s on the radial component for both VSC and GRB (corresponding to the FAS peak at 0.8 Hz), and the much bigger difference in the PSA for the radial and transverse components at GRB than at VSC. Note that the PSA for GRB has a relatively broadband plateau from about 0.3 to 1.3 s, with local peaks superimposed on the plateau, whereas the PSA for VSC is more sharply peaked near 1.25 s.

The lower graph in Figure 11 contains the PSA for three other recordings of the L'Aquila mainshock, in addition to that at GRB. These stations (ASS, CDS, and CSS) were chosen because they are at a similar distance from the earthquake, as is GRB (the distances and azimuths are given in the Fig. 11 legend; note that the azimuths are very different than that to GRB). According to Pacor *et al.* (2011), each of the three stations falls in the same site class as GRB, with an estimated V_{S30} value of 900 m/s (there are no other recordings in the 80–110 km distance range with V_{S30} as low as that for VSC, and therefore we only show comparisons of other recordings with GRB). The PSA from ASS, CDS, and CSS have been adjusted to a distance of 98 km and a V_{S30} of 631 m/s (the values for GRB) using the Boore and Atkinson (2008; the updated GMPE is hereafter referred to as BA08) GMPEs. The distance term in the BA08 GMPEs have been modified using Scasserra *et al.* (2009) adjustments (those adjustments were derived using data from Italian earthquakes obtained before the L'Aquila sequence). We used the BA08 V_{S30} adjustments because they are generally in the middle of those from the Pacific Earthquake Engineering Research Center Next Generation Attenuation (PEER NGA) GMPEs. At periods less than about 0.3 s, the PSA from the three added stations are similar to that from GRB, and all are somewhat lower than at VSC. For periods around 1 s, the PSA from the three stations are significantly lower than the PSA from the recordings at GRB.

Figure 11 also compares the PSA from recordings at VSC and GRB with the PSA from the median predictions from four PEER NGA GMPEs, as well as the \pm one standard deviation bounds for the Abrahamson and Silva (2008) PEER NGA model. Shown in the figure are the medians from the published GMPEs, as well as those after applying the Scasserra *et al.* (2009) distance modifications. The comparison between observed and predicted spectra should be with GMRotI50 (the heavy black line), as that is the measure predicted by the NGA GMPEs. The most obvious conclusion is that the shapes of the PSAs from the L'Aquila mainshock

recordings are quite different from the GMPE predictions. At short periods (less than about 0.3 s) the observed PSA values are generally lower than those from GMPEs (the exception being those from the modified AS08 and CY08 GMPEs). Perhaps the most important conclusion from the comparisons in Figure 11 is that the PSA at periods near 1 s from both GRB and VSC are significantly greater than those from the GMPEs (and from the L'Aquila recordings away from Rome, as noted in the previous paragraph). While we should not expect the motions from a few recordings of a single earthquake to be close to the median values from a large global dataset, we think it significant that the observed motions at both GRB and VSC exceed the median plus one standard deviation predictions from the GMPEs.

Ameri *et al.* (2009), Pacor *et al.* (2011), and Massa *et al.* (2012) also compare the L'Aquila response spectra with other GMPEs, including the BA08 GMPEs and several others based on global as well as Italian-only data. They do not include a distance modification for BA08. These authors also find that all of the considered GMPEs overestimate the L'Aquila response spectra at short periods. In contrast, they find that the motions from the GMPEs and from the many recordings of the L'Aquila mainshock taken as a whole are similar for longer periods.

Discussion and Conclusions

The 2009 L'Aquila earthquake and its aftershock sequence provided the first-ever recordings of earthquake ground shaking in the urban area of Rome. We study the recordings from three stations: one station (GRB) is on relatively stiff volcanic deposits in an upland area, and the other two stations are several kilometers away, in the Tiber River valley, at a site underlain by soft sediments. Of these latter two stations, one is at the ground surface (VSC) and one is in a borehole 72 m beneath the surface (BRH). The VSC and BRH records show that there are significant resonance amplifications, with a fundamental mode frequency near 1 Hz and a number of higher modes at higher frequencies. The frequencies of these modes and the relative amplitudes of the VSC and BRH motions are in good agreement with theoretical predictions, which use velocities measured in the borehole. In spite of the good agreement with theoretical predictions, however, it is clear that there are complexities in the polarization of motions at VSC near the fundamental mode frequency, with the expected linear polarization in a radial-component direction becoming elliptically polarized. In contrast, the motions at GRB show the expected linear polarization for the strongest motions, in agreement with the radiation pattern of the source. There is a peak in the GRB motion, however, at a frequency close to the fundamental mode frequency at VSC. HVSRs (from the mainshock, an average of nine aftershocks, and from ambient noise) show peaks at GRB and VSC, near 1 Hz, with that at GRB being at a somewhat higher frequency than at VSC. If this peak corresponds to a site resonance, it is not predicted by the

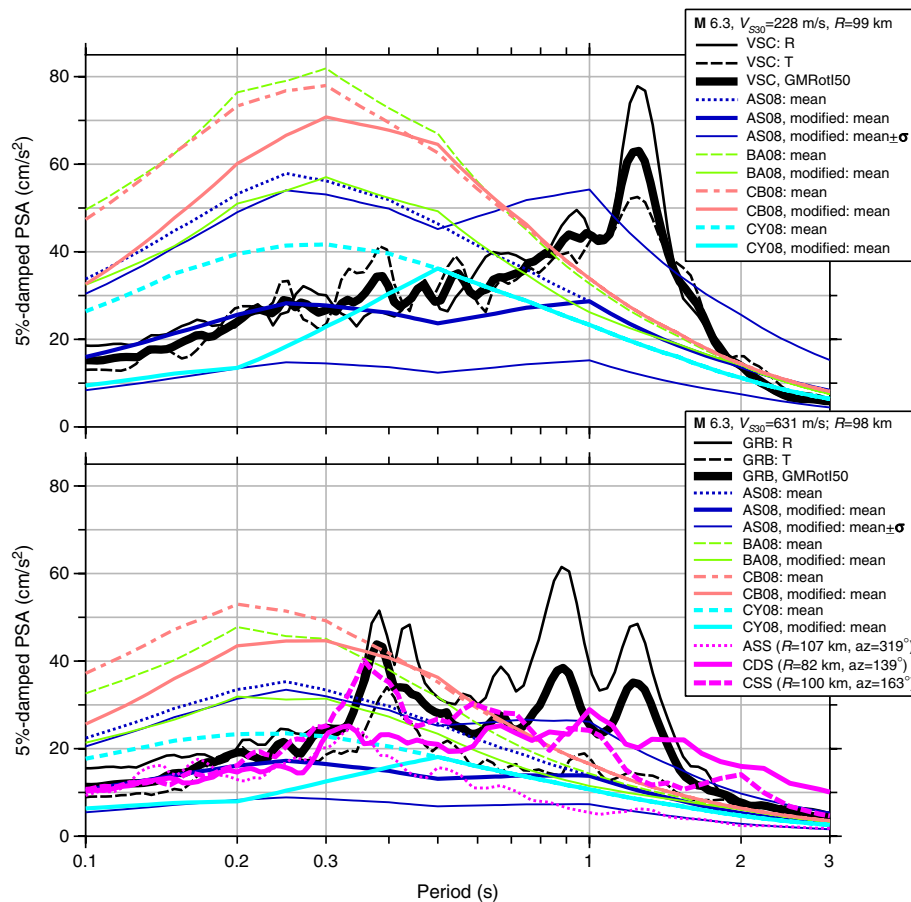


Figure 11. PSA at VSC (top) and GRB (bottom) compared with predictions from four PEER NGA models (AS08: Abrahamson and Silva, 2008); BA08: Boore and Atkinson, 2008; CB08: Campbell and Bozorgnia, 2008; CY08: Chiou and Youngs, 2008), modified using the Scasserra et al. (2009) distance modifications. In the figure legend, “mean” is actually $\exp(\ln \text{PSA})$ and “mean $\pm \sigma$ ” is $\exp(\ln \text{PSA} \pm \sigma)$, where $\ln \text{PSA}$ is the mean value of $\ln \text{PSA}$ given by the GMPE. Also shown are the geometric means of the PSA computed for horizontal component recordings of the mainshock at three stations located approximately the same distance from the source as Rome (98 km), but at different azimuths (given in the legend, clockwise from north; the azimuth to Rome is 237°); these PSAs have been adjusted to $V_{S30} = 631$ m/s (see text). The distances and azimuths are computed from point “PA” in figure 18 of Herrmann et al. (2011), as an approximation of the center of moment release. The color version of this figure is available only in the electronic edition.

velocity model we have estimated for GRB; although we have no velocity measurements at this station, it is outside of the Tiber River valley, and thus is not underlain by the relatively low-velocity Holocene sediments that lead to the 1 Hz resonance at VSC. The amplification at GRB is unlikely to be due to the source, because GRB is essentially perpendicular to the direction of fault rupture, the increased motions are not present at the other three stations away from Rome that recorded the mainshock, and the amplification appears on the noise HVSr. Although the agreement of the observed and predicted site response of VSC relative to GRB is not as good as the VSC/BRH response, both the observed and predicted FAS at VSC relative to that at GRB show a peak near 1 Hz, with the motion at VSC being larger than the motion at GRB by a factor of about 2 to 3. The complications in the waveforms at the Tiber River valley site, as well as the unexpected apparent site amplification near 1 s at the stiffer upland site, caution against using simple

one-dimensional site amplification predictions and against using ratios of motions from nearby sites to estimate the station-specific amplification (relative to the motion of the incoming waves below the site).

The observed response spectra from the mainshock exceed the one-standard-deviation bounds from recent GMPEs based on a global database, for periods around 1 s. The response spectra near 1 s also exceed those from other stations at similar distances and site conditions as GRB, but at different azimuths. At shorter periods, the observed response spectra are within the one-standard-deviation bounds of several GMPEs (adjusted to account for differences in distance attenuation between the global dataset and Italian data), but they are lower than those from other GMPEs.

In summary, the mainshock and aftershock motions, as well as ambient noise, recorded at a station in the Tiber River valley (VSC) all agree that there is a pronounced amplification near the theoretically predicted frequency of 1 Hz. There

is also a smaller amplification, of unknown origin, at a somewhat higher frequency than 1 Hz at a nearby upland site (GRB). The motion near 1 Hz at GRB is greater than for other recordings away from Rome (there are no recordings away from Rome at distances comparable to the Rome–L'Aquila distances for sites underlain by the velocities similar to those at VSC, so we can only compare other recordings with those at GRB). The motions near 1 Hz at both VSC and GRB exceed the mean-plus-one-standard-deviation motions from a large global dataset.

Data and Resources

The seismic data used in this article are part of the database of the ongoing Project FIRB/MIUR-Abruzzo; although not publically available at present, they will be available at the end of that project. The site amplifications were computed using the programs *nrattle* and *roll* (written by C. Mueller; *nrattle* was revised by R. Herrmann), available as part of the SMSIM package of programs; the programs are included in SMSIM with their permission. The latest version of SMSIM can be obtained from the online software link on <http://www.daveboore.com> (last accessed April 2012); the use of the SMSIM programs is described in Boore (2005). Hypocenters are from the INGV bulletin (at <http://iside.rm.ingv.it>; last accessed July 2011). Moment magnitudes *M* from the USGS catalog (<http://earthquake.usgs.gov/earthquakes/eqarchives/sopar/> (last accessed February 2012) are available for the two largest shocks.

The notes http://www.daveboore.com/daves_notes/daves_notes_on_poissons_ratio.pdf (last accessed January 2013) and http://www.daveboore.com/daves_notes/daves_notes_on_relating_density_to_velocity_v1.2.pdf (last accessed January 2013) referred to in Appendix A are available upon request from the second author of this article.

Acknowledgments

Seismograms used in this study were collected thanks to funds provided by the projects FIRB 2002-2205 (code: RBAU01JMT3) and COFIN 2004-2005 (code: 2004041297_002). The authors wish to thank Francesco Basile for his help in the field. We benefited from conversations with and Giovanna Calderoni, Fabrizio Cara, Giuliana Mele, Carlo Meletti, Giuliano Milana, Ivo Oprsal, Shri K. Singh, Chris Stephens, and Jiri Zahradnik, all of whom provided useful suggestions for our work. Part of the research activities were carried on by one of the authors (A.C.) for his PhD thesis at the Charles University in Prague (Czech Republic), with support from the projects GACR 205/07/0502 and MSM 0021620860. We thank Gabriele Ameri, Joe Fletcher, William Stephenson, and an anonymous reviewer for their thoughtful and constructive reviews of the manuscript.

References

- Abrahamson, N. A., and W. J. Silva (2008). Summary of the Abrahamson & Silva NGA ground-motion relations, *Earthq. Spectra* **24**, 67–97.
- Ambrosini, S., S. Castenetto, F. Cevolani, E. Di Loreto, R. Funicello, L. Liperi, and D. Molin (1986). Risposta sismica dell'area urbana di Roma in occasione del terremoto del Fucino del 13-1-1915, *Mem. Soc. Geogr. Ital.* **35**, 445–452 (in Italian).
- Ameri, G., M. Massa, D. Bindi, E. D'Alema, A. Gorini, L. Luzi, S. Marzorati, F. Pacor, R. Paolucci, R. Puglia, and C. Smerzini (2009). The 6 April 2009 M_w 6.3 L'Aquila (central Italy) earthquake: Strong-motion observations, *Seismol. Res. Lett.* **80**, 951–966.
- Bindi, D., S. Parolai, M. Picozzi, and A. Ansal (2010). Seismic input motion determined from a surface—Downhole pair of sensors: A constrained deconvolution approach, *Bull. Seism. Soc. Am.* **100**, 1375–1380, doi: [10.1785/0120090306](https://doi.org/10.1785/0120090306).
- Bonnefoy-Claudet, S., A. Kohler, C. Cornou, M. Whatelet, and P.-Y. Bard (2008). Effects of Love waves on microtremor H/V ratio, *Bull. Seismol. Soc. Am.* **98**, 288–300.
- Boore, D. M. (2004). Can site response be predicted? *J. Earthq. Eng.* **8**, Special Issue 1, 1–41.
- Boore, D. M. (2005). SMSIM—Fortran Programs for simulating ground motions from earthquakes: Version 2.3—A revision of OFR 96-80-A, *U.S. Geol. Surv. Open-File Rept. 00-509*, revised 15 August 2005, 55 pp., available through <http://www.daveboore.com> (last accessed April 2012).
- Boore, D. M., and G. M. Atkinson (2008). Ground-motion prediction equations for the average horizontal component of PGA, PGV, and 5%-damped PSA at spectral periods between 0.01 s and 10.0 s, *Earthq. Spectra* **24**, 99–138.
- Boore, D. M., and W. B. Joyner (1991). Estimation of ground motion at deep-soil sites in eastern North America, *Bull. Seismol. Soc. Am.* **81**, 2167–2185.
- Boore, D. M., J. Watson-Lamprey, and N. A. Abrahamson (2006). Orientation-independent measures of ground motion, *Bull. Seismol. Soc. Am.* **96**, 1502–1511.
- Boschi, E., A. Caserta, C. Conti, M. Di Bona, R. Funicello, L. Malagnini, F. Marra, G. Martines, A. Rovelli, and S. Salvi (1995). Resonance of subsurface sediments—An unforeseen complication for designers of Roman columns, *Bull. Seismol. Soc. Am.* **85**, 320–324.
- Bozzano, F., A. Andreucci, M. Gaeta, and R. Salucci (2000). A geological model of the buried Tiber River valley beneath the historical centre of Rome, *Bull. Eng. Geol. Env.* **59**, 1–21.
- Bozzano, F., A. Caserta, A. Govoni, F. Marra, and S. Martino (2008). Static and dynamic characterization of alluvial deposits in the Tiber River Valley: New data for assessing potential ground motion in the City of Rome, *J. Geophys. Res.* **113**, B01303, doi: [10.1029/2006JB004873](https://doi.org/10.1029/2006JB004873).
- Brocher, T. M. (2005). Empirical relations between elastic wavespeeds and density in the Earth's crust, *Bull. Seismol. Soc. Am.* **95**, 2081–2092.
- Brocher, T. M. (2008). Compressional and shear-wave velocity versus depth relations for common rock types in northern California, *Bull. Seismol. Soc. Am.* **98**, 950–968, doi: [10.1785/0120060403](https://doi.org/10.1785/0120060403).
- Campbell, K. W., and Y. Bozorgnia (2008). NGA ground motion model for the geometric mean horizontal component of PGA, PGV, PGD and 5% damped linear elastic response spectra for periods ranging from 0.01 to 10 s, *Earthq. Spectra* **24**, 139–171.
- Caserta, A., S. Martino, F. Bozzano, A. Govoni, and F. Marra (2012). Dynamic properties of low velocity alluvial deposits influencing seismically-induced shear strains: The Grottaperfetta valley test-site (Rome, Italy), *Bull. Earthq. Eng.* doi: [10.1007/s10518-012-9349-8](https://doi.org/10.1007/s10518-012-9349-8).
- Chávez-García, F. J., D. Raptakis, K. Makra, and K. Pitilakis (2000). Site effects at Euro-seistest-II. Results from 2D numerical modelling and comparison with observations, *Soil Dynam. Earthq. Eng.* **19**, 23–39.
- Chiou, B. S. J., and R. R. Youngs (2008). An NGA model for the average horizontal component of peak ground motion and response spectra, *Earthq. Spectra* **24**, 173–215.
- Cifelli, F., S. Donati, F. Funicello, and A. Tertulliani (2000). High-density macroseismic survey in urban areas. Part 2: Results for the city of Rome, Italy, *Bull. Seismol. Soc. Am.* **90**, 298–311.
- Cinti, F. R., F. Marra, F. Bozzano, F. Cara, G. Di Giulio, and E. Boschi (2008). Tectonostratigraphic investigations within a highly urbanized area: The case of the Grottaperfetta valley in the city of Rome (Italy), *Ann. Geophys.* **51**, no. 5/6, 849–865.

- Fäh, D., C. Iodice, P. Suhadolc, and G. F. Panza (1993). A new method for the realistic estimation of seismic ground motion in megacities: The case of Rome, *Earthq. Spectra* **9**, 643–668.
- Fäh, D., F. Kind, and D. Giardini (2001). A theoretical investigation of average H/V ratios, *Geophys. J. Int.* **145**, 535–549.
- Florindo, F., D. B. Karner, F. Marra, P. R. Renne, A. P. Roberts, and R. Weaver (2007). Radioisotopic age constraints for glacial terminations IX and VII from aggradational sections of the Tiber River delta in Rome, Italy, *Earth Planet. Sci. Lett.* **256**, 61–80.
- Funicello, R., and M. Parotto (1978). Il substrato sedimentario nell'area dei Colli Albani: considerazioni geodinamiche e paleogeografiche sul margine tirrenico dell'Appennino centrale, *Geol. Romana* **17**, 233–287 (in Italian).
- Herrmann, R., L. Malagnini, and I. Munafò (2011). Regional moment tensors of the 2009 L'Aquila earthquake sequence, *Bull. Seismol. Soc. Am.* **101**, 975–993, doi: [10.1785/0120100184](https://doi.org/10.1785/0120100184).
- Joyner, W. B., R. E. Warrick, and A. A. Oliver III (1976). Analysis of seismograms from a downhole array in sediments near San Francisco Bay, *Bull. Seismol. Soc. Am.* **66**, 937–958.
- Karner, D. B., and F. Marra (1998). Correlation of fluviodeltaic aggradational sections with glacial climate history: A revision of the classical Pleistocene stratigraphy of Rome, *Geol. Soc. Am. Bull.* **110**, 748–758.
- Karner, D. B., F. Marra, and P. Renne (2001). The history of the Monti Sabatini and Alban Hills volcanoes: Groundwork for assessing volcanic-tectonic hazards for Rome, *J. Volcanol. Geoth. Res.* **107**, 185–219.
- Kinoshita, S. (2010). A method for estimating the Green's Function of a near-surface layer for SH-waves by means of a borehole receiver array, *Bull. Seismol. Soc. Am.* **100**, 1381–1388, doi: [10.1785/0120090115](https://doi.org/10.1785/0120090115).
- Konno, K., and T. Ohmachi (1998). Ground-motion characteristics estimated from spectral ratio between horizontal and vertical components of microtremor, *Bull. Seismol. Soc. Am.* **88**, 228–241.
- Lermo, J., and F. J. Chávez-García (1993). Site effect evaluation using spectral ratios with only one station, *Bull. Seismol. Soc. Am.* **83**, 1574–1594.
- Marra, F., and C. Rosa (1995). Stratigrafia e assetto geologico dell'area romana, in "La Geologia di Roma. Il Centro Storico", *Memorie Descrittive della Carta Geologica d'Italia (special issue)* **50**, 49–118 (in Italian).
- Marra, F., F. Florindo, and E. Boschi (2008). The history of glacial terminations from the Tiber River (Rome): Insights to glacial forcing mechanisms, *Paleoceanography* **23**, PA2205, doi: [10.1029/2007PA001543](https://doi.org/10.1029/2007PA001543).
- Massa, M., L. Luzi, F. Pacor, D. Bindi, and G. Ameri (2012). Comparison between empirical predictive equations calibrated at global and national scale and Italian strong-motion data, *Boll. Geof. Teor. Appl.* **53**, 37–53.
- Moczo, P., A. Rovelli, P. Labák, and L. Malagnini (1995). Seismic response of the geologic structure underlying Roman Colosseum and a 2D resonance of a sediment valley, *Ann. Geofisc.* **38**, no. 5–6, 939–956.
- Olsen, K. B., A. Akinci, A. Rovelli, F. Marra, and L. Malagnini (2006). 3D ground-motion estimation in Rome, Italy, *Bull. Seismol. Soc. Am.* **96**, 133–146.
- Pacor, F., G. Ameri, D. Bindi, L. Luzi, M. Massa, R. Paolucci, and C. Smerzini (2011). Characteristics of strong ground motions from the L'Aquila ($M_w = 6.3$) earthquake and its strongest aftershocks, *Boll. Geof. Teor. Appl.* **52**, 471–490.
- Pagliaroli, A., B. Quadrio, T. Sanò, F. Sabetta, S. Castenetto, G. Naso, M. Moscatelli, G. Lanzo, and V. Di Fiore (2011). Risposta sismica locale dell'area archeologica comprendente il Colle Palatino, i Fori e il Colosseo, in *Roma archaeologia. Interventi per la tutela e la fruizione del patrimonio archeologico; terzo rapporto*, R. Cecchi (Editor), Mondadori Electa S.p.A., Milano, 90–119 (in Italian).
- Rovelli, A., A. Caserta, L. Malagnini, and F. Marra (1994). Assessment of potential strong motions in the city of Rome, *Ann. Geofisc.* **37**, 1745–1769.
- Rovelli, A., L. Malagnini, A. Caserta, and F. Marra (1995). Using 1-D and 2-D modelling of ground motion for seismic zonation criteria: Results for the city of Rome, *Ann. Geofisc.* **38**, 591–605.
- Sbarra, P., V. De Rubeis, E. Di Luzio, M. Mancini, M. Moscatelli, F. Stigliano, P. Tosi, and R. Vallone (2012). Macroseismic effects highlight site response in Rome and its geological signature, *Nat. Hazards* **62**, 425–443, doi: [10.1007/s11069-012-0085-9](https://doi.org/10.1007/s11069-012-0085-9).
- Scasserra, G., J. P. Stewart, P. Bazzurro, G. Lanzo, and F. Mollaioli (2009). A comparison of NGA ground-motion prediction equations to Italian data, *Bull. Seismol. Soc. Am.* **99**, 2961–2978.
- Shearer, P. M., and J. A. Orcutt (1987). Surface and near-surface effects on seismic waves—Theory and borehole seismometer results, *Bull. Seismol. Soc. Am.* **77**, 1168–1196.
- Signorini, R. (1939). Risultati geologici della perforazione eseguita dall'A.G.I.P. alla Mostra autarchica del Minerale nel Circo Massimo di Roma, *Boll. Soc. Geol. Ital.* **58**, 60–63 (in Italian).

Appendix A

Velocity, Density, and Q Models for Computed Response

The shear-wave velocities, depths, and lithology shown in Figure 2 are based on several boreholes (in particular, the one near VSC, from which seismic velocities were measured), as well as general experience from extensive geologic work in the area of Rome; the primary references used in constructing Figure 2 are Signorini (1939), Bozzano *et al.* (2008), Cinti *et al.* (2008), and Pagliaroli *et al.* (2011). For the purpose of computing site response at VSC and GRB, we need models of both shear-wave (V_S) and compressional-wave (V_P), velocity, density, and Q as a function of depth.

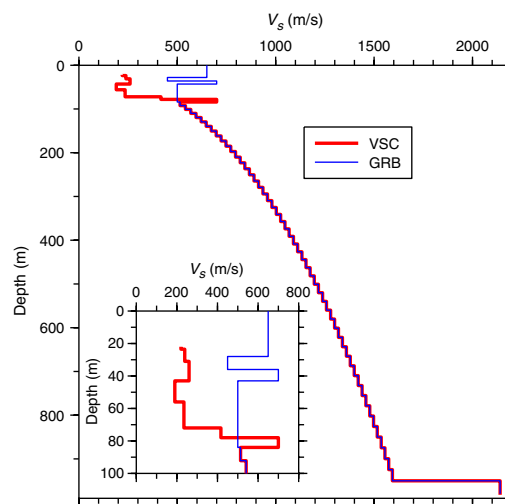


Figure A1. Velocity models used for the theoretical amplification calculations (the inset graph shows the models in the upper 100 m). The starting depth of the VSC model has been adjusted to make it clear that the velocities under both VSC and GRB are assumed to be the same below about 100 m. This assumption is physically plausible and simplifies the computation of the theoretical VSC/GRB spectral ratio. This ratio is computed as the ratio of the site responses at the individual stations relative to motions on various equivalent half-spaces (see text). The color version of this figure is available only in the electronic edition.

The measurements of [Bozzano et al. \(2008\)](#) at VSC, with slight adjustments, were used to provide V_S to depths of about 62 m. At GRB the velocities down to 43 m are based on general experience of the correlations of velocity and lithology. At greater depths below both VSC and GRB, a power-law gradient model was constructed subject to the constraints shown in Figure 2 that V_S be 500 and 1600 m/s at depths of 84 and 950 m below GRB, respectively. These constraints are based on judgement from several of the authors of this article. The continuous V_S from the power law were converted to a multilayer, constant velocity model using the SMSIM program *pwr2lyr*, which ensures that the travel time across the constant velocity layer equals that for the power law over the same depth range. The half-space V_S of 2140 m/s is taken from [Herrmann et al. \(2011\)](#).

The V_P velocities at shallow depths beneath VSC are taken from an unpublished study by one of this article's authors. At deeper depths below VSC and at all depths below GRB a mapping between V_P and V_S was used, according to this algorithm:

- for material above the water table:

$$V_P = 2.08V_S \quad (\text{A1})$$

- for material below the water table:

$$V_P = \begin{cases} 1500, & V_S \leq 187.5 \\ 363.2V_S^{0.271}, & 187.5 < V_S \leq 808.4 \\ 940.9 + 2.0947V_S - 8.206 \times 10^{-4}V_S^2, & 808.4 < V_S \\ + 2.683 \times 10^{-7}V_S^3 - 2.51 \times 10^{-11}V_S^4, & \end{cases} \quad (\text{A2})$$

The units of velocity in equations (A1) and (A2) are m/s. This algorithm is based on the relations between measured

V_P and V_S contained in unpublished notes of one of the authors (DMB, *daves_notes_on_poisson's_ratio.pdf*; see [Data and Resources](#) for availability). Equation (A1) is based on an assumed Poisson's ratio of 0.35. The last relation in equation (A2) (for $808.4 < V_S$) is from equation (9) in [Brocher \(2005\)](#), with units converted to m/s for velocity.

For density we used the algorithm given on pp. 10 and 11 of *daves_notes_on_relatng_density_to_velocity_v1.pdf* (see [Data and Resources](#) for availability). For Q we used equations (19)–(21) of [Brocher \(2008\)](#).

The models used in the site-response calculations are given in the  electronic supplement. The models are plotted in Figure A1.

Istituto Nazionale di Geofisica e Vulcanologia
Via di Vigna murata 605
00143 Roma, Italy
(A.C., A.R., A.G., F.M.)

U.S. Geological Survey
MS 977, 345 Middlefield Road
Menlo Park, California 94025
boore@usgs.gov
(D.M.B.)

Department of Physics
Università degli Studi Roma TRE
Via della Vasca Navale 84
00146 Roma, Italy
(G.D.)

Department of Physics/Sector of Geophysics Via Berti Pichat 6/2
University of Bologna
40127 Bologna, Italy
(E.B.)

Manuscript received 24 April 2012